PNAS Nexus

PNAS Nexus, 2022, **1**, 1–9
https://doi.org/10.1093/pnasnexus/pgac272
Advance access publication date: 7 December 2022
Research Report

Malaria absorption peaks acquired through the skin of patients with infrared light can detect patients with varying parasitemia

Gabriela A. Garcia[a], Tharanga N. Kariyawasam[b], Anton R. Lord[c], Cristiano Fernandes da Costa[d], Lana Bitencourt Chaves[e], Josué da Costa Lima-Junior[e], Rafael Maciel-de-Freitas[a,f,1] and Maggy T. Sikulu-Lord[b,*,1]

[a]Laboratório de Transmissores de Hematozoários, Instituto Oswaldo Cruz, Fiocruz, Rio de Janeiro, RJ 21040-900, Brazil
[b]School of Biological Sciences, Faculty of Science, The University of Queensland, Brisbane, QLD 4072,, Australia
[c]School of Computer Science, Centre for Data Science, Queensland University of Technology, Brisbane, QLD 4000, Australia
[d]Fundação de Vigilância em Saúde, Manaus, AM 69093-018, Brazil
[e]Laboratório de Imunoparasitologia, Instituto Oswaldo Cruz, Fiocruz, Rio de Janeiro, RJ 21040-900, Brazil
[f]Department of Arbovirology, Bernhard Nocht Institute for Tropical Medicine, Bernhard-Nocht-Straße 74, 20359 Hamburg, Germany
*To whom correspondence should be addressed: Email: maggy.lord@uq.edu.au
[1]R.M-d.-F. and M.T.S.-L. equally contributed to this work.
Edited By: Richard Stanton

Abstract

To eliminate malaria, scalable tools that are rapid, affordable, and can detect patients with low parasitemia are required. Non-invasive diagnostic tools that are rapid, reagent-free, and affordable would also provide a justifiable platform for testing malaria in asymptomatic patients. However, non-invasive surveillance techniques for malaria remain a diagnostic gap. Here, we show near-infrared *Plasmodium* absorption peaks acquired non-invasively through the skin using a miniaturized hand-held near-infrared spectrometer. Using spectra from the ear, these absorption peaks and machine learning techniques enabled non-invasive detection of malaria-infected human subjects with varying parasitemia levels in less than 10 s.

Significance Statement

We provide a report of the application of the near-infrared spectroscopy (NIRS) technique and machine learning algorithms for non-invasive and reagent-free detection *Plasmodium vivax* and *Plasmodium falciparum* infected patients with varying parasitemia levels. The technique involves a 5 to 10 s interaction of harmless infrared light with the skin of human subjects and subsequent collection of a diagnostic spectral signature. NIRS is portable, results can be achieved in real time and it has the capacity to screen thousands of people in a day without consuming any reagents. It is an ideal surveillance tool for screening a large population of people to identify infected populations with minimal cost and time and can easily be scaled up to guide current malaria elimination strategies.

Introduction

In 2021, the World Health Organization (WHO) estimated that 241 million malaria-related cases and 627,000 malaria-related deaths occurred in 2020 [1]. The *Plasmodium* parasites that cause the disease are transmitted to people by bites of infected female *Anopheles* mosquitoes. Among them, the two major *Plasmodium* parasite species are *Plasmodium falciparum* and *P. vivax*. In 2020, *P. falciparum* accounted for 98% of estimated malaria cases globally and 99.7% of the cases were reported in the WHO African region. In the WHO region of Americas, *P. vivax* is the predominant parasite representing 68% of malaria cases in the region [1]. In 2015, WHO set a strategy to guide countries toward malaria elimination by reducing global malaria incidences and mortality by at least 90% and eliminating malaria in at least 35 countries by the year 2030 [2]. One of the pillars on which this strategy is based on is to ensure universal access to malaria prevention, diagnosis, and treatment. To achieve this target, WHO recommends universal testing of all suspected cases of malaria. This is particularly crucial in endemic areas where a majority of the malaria-infected population can be asymptomatic [3] as well as in low malaria transmission settings where the proportion of asymptomatic population among the infected individuals can be as high as 60% [4]. Universal testing is expected to prompt and facilitate the treatment of asymptomatic population to limit further community transmission.

Optical microscopy, rapid diagnostic tests (RDTs), and molecular tests are the three main diagnostic techniques currently available for malaria diagnosis. Microscopy is the traditional way of detecting malaria parasites in stained thick or thin peripheral blood films using Giemsa, Wright's, or Field's stains. Thick blood films are used to detect the presence of malaria parasite, whereas thin

Competing Interest: The authors declare no competing interest.
Received: September 29, 2022. **Accepted:** December 5, 2022

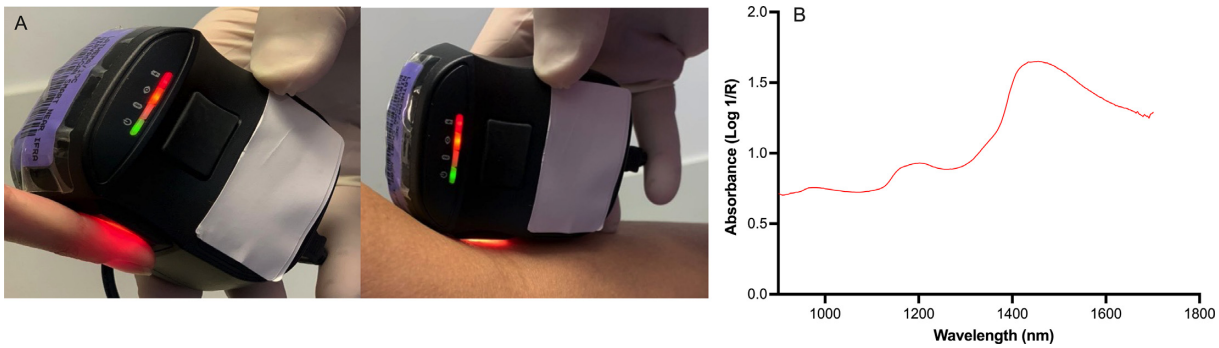

Figure 1. An illustration of non-invasive scanning of the finger and the arm with the NIRvascan spectrometer (A) and reflective spectrum produced from the scanning (B).

blood films are often used to confirm the *Plasmodium* species [5]. It is the most widely used technique for malaria diagnosis due to its low cost, simplicity, and its capacity to detect parasites, differentiate *Plasmodium* species, and estimate the parasite concentration. However, microscopy is technically demanding, time-consuming, and requires specialized expertise to accurately identify parasites and differentiate species in samples with low parasitemia or samples with mixed infections [6–8]. As the average microscopist detection limits are estimated to be 50 to 100 parasites/μL, the likelihood of underestimating infection rates particularly in low transmission settings or among asymptomatic population where parasitemia is low has been reported [9]. Microscopy is also often unavailable in rural settings where power supply can be problematic [10].

RDTs detect malaria antigens in blood by targeting *Plasmodium*-specific proteins such as histidine-rich protein II (HRP-II) or lactate dehydrogenase (LDH) [11, 12]. RDTs are simple, relatively cheap, and can be used in remote areas without specialized equipment or need for electricity. However, RDTs can only reliably detect 50 to 100 parasites/μL [11, 12], they have to be coupled with other techniques in areas where more than one malaria parasite species is present due to their inability to differentiate *Plasmodium* species [9, 13], and they can generate false positives due to the persistence of HRP-II following an infection [14].

Molecular tests such as polymerase chain reaction (PCR) are currently the most accurate and the most sensitive techniques for detecting malaria in low- or sub-microscopic samples, for mixed infections, and for differentiating *Plasmodium* species [15–17]. However, molecular techniques are costly, time-consuming, and require skilled expertise [18]. In addition, none of these traditional techniques are equipped for large-scale surveillance of malaria cases in endemic countries.

Here, we explored the potential of a miniaturized near-infrared spectrometer that could easily be scaled up for universal surveillance of malaria cases to guide the proposed WHO malaria elimination strategy. The near-infrared spectroscopy (NIRS) is a simple to use, non-invasive, reagent-free technique that uses the near-infrared part of the electromagnetic spectrum to characterize biological samples. It involves shining a beam of light on a sample for approximately 5 s and subsequent collection of a spectral signature. The spectral signature is a reflection of the chemical composition of a sample and can be analyzed using machine learning algorithms to identify diagnostic features. We hypothesized that the presence of malaria parasites in red blood cells can produce unique infrared signatures that could potentially be used for diagnosis of malaria. We used a handheld spectrometer to non-invasively collect spectral signatures from the right and left ears, arms, and fingers of malaria-positive and -negative individuals living in a malaria-endemic area in Brazil where both *P. falciparum* and *P. vivax* are prevalent at a 30%/70% ratio.

Materials and Methods

Study area, population, and malaria prevalence

The study was conducted in the municipality of São Gabriel da Cachoeira (SGC), located in the Upper Rio Negro region, State of Amazonas, northern Brazil (0°07′51″S; 67°05′15″W). SCG is surrounded by the Amazon and is the municipality with the highest percentage of self-declared indigenous people (over 75%) in Brazil, with an estimated 30,000 people living in the area, and over 20 ethnic groups [19]. The Amazon region represents 99.8% of all malaria cases in Brazil and cases of both *P. vivax* and *P. falciparum* have been recorded. In 2019, a total of 8,605 cases were reported in SCG, and from January 2019 to June 2020, an estimated 34% of malaria cases were caused by *P. falciparum* and mixed infections [20].

Ethics approval

The study was approved by the human ethics committee of Instituto Oswaldo Cruz (Ethics Protocol No. 94,070,418.7.0000.5248). Patients with malaria symptoms who were seeking diagnosis and treatment at the basic health units were approached to volunteer for this study. Prior to recruitment, a written informed consent was obtained from patients after the nature and possible consequences of the studies were explained. The written consent form was previously approved by human ethics committee at Fiocruz. Further work to determine presence of malaria parasites in volunteer's blood was approved by the National Genetic Heritage Management System (A88B262).

NIRS instrument used

NIRvascan near-infrared spectrometer reflective model G1 (Allied Scientific Pro, Canada) was used in this study (Fig. 1). The model used is a diffuse reflectance spectrometer with wavelength ranging from 900 to 1700 nm, a 5000:1 signal-to-noise ratio, and an optical resolution of 10 nm pixel resolution. It has an inGaAs detector (Hamamatsu model G12180-010A), a dark current of 0.8nA @VR = 1 V, noise equivalent power of 1.4×10^{14} @λp, and a light source with two integrated tungsten halogen lamps of 1 W, built-in at 45° from the surface. It weighs 136 g and measures 82.2 × 63 × 40 mm. The spectrometer is rechargeable and can be operated by either a computer or a smartphone via Bluetooth.

Scanning

Participants presenting with malaria symptoms were scanned with the NIRvascan spectrometer, which was connected to a notebook using Bluetooth. The participants left and right arm, ear, and finger were one after the other placed directly onto the spectrometer's scan window and spectra was collected by pressing the scan button. Two spectra were collected from each body part scanned. A total of 60 patients were scanned and a total of 360 spectra were collected. In addition, 1 mL of whole blood was collected intravenously from each patient into EDTA tubes and stored for microscopy and PCR. Patient metadata, including gender, age, weight, skin color, and height were also recorded. An example of a raw spectrum collected by the NIRvascan spectrometer is shown in Fig. 1.

Gold standard microscopy and PCR confirmation of malaria-positive and malaria-negative cases

To validate NIR technique's capacity to differentiate infected from uninfected subjects, differentiate *Plasmodium* species and determine parasitemia level of subjects, the WHO gold standard technique of blood films, and microscopy was used.

Blood films were read by at least two microscopists. Readings were averaged, and quality assurance was provided by a WHO Level 1 certified malaria microscopist. Microscopy results were grouped into four levels of parasitemia groups; high parasitemia (>100,000 parasites/μL); moderate parasitemia (10,000 to 100,000 parasites/μL); low parasitemia (500 to 10,000 parasite/μL); and very low parasitemia (300 to 500 parasites/μL).

The infection status and *Plasmodium* species type were further confirmed by standard PCR. Genomic DNA from whole blood samples were extracted using the QIAamp DNA Blood Mini Kit according to the manufacturer's instructions (Qiagen, Hilden, Germany) and stored at −20°C until amplification. Detection and identification of *Plasmodium* species was performed using Nested PCR with specific primers for genus (*Plasmodium* sp.) and species (*P. falciparum* and *P. vivax*) as described by Snounou et al. [21, 22]. In the first amplification reaction, 3 μL of purified genomic DNA were used in a 25 μL reaction with genus specific primers. During the second PCR reaction, 3 μL of PCR amplification product of the first reaction was used as a template in a 25 μL reaction with species specific primers. The amplified PCR products were size-fractionated by electrophoresis in 2% agarose gel (Sigma Aldrich, Missouri, MO, USA), 1 × TAE buffer (0.04 M TRIS-acetate, 1 mM EDTA) in the presence of 1 × GelRed nucleic acid stain (Biotium, Fremont, CA, USA). PCR products were visualized by ultraviolet (UV) illumination. The species of *Plasmodium* were determined by species-specific amplicon sizes.

Data analysis

Savitzky-golay least-square filtering

To determine unique absorption peaks for malaria parasites, all spectra from malaria-infected subjects were averaged based on the body part scanned regardless of the *Plasmodium* species they were infected with and compared against averaged spectra of uninfected subjects. To identify absorption peaks for *P. falciparum* and *P. vivax*, raw spectra of each species were averaged separately.

To smoothen the signal and provide a better visualisation of the important peaks, Savitzky–Golay (SG) smoothing filters were used. When coefficients of SG filter are performed on NIR signal using weighted moving average, a polynomial P of the degree k is fitted to a window size using the formular;

$$N = N_r + N_l + 1,$$

where, N is the window size, N_r and N_l are signal points on the right and left of the current signal, respectively [23]. Least-squares smoothing digital filters with 15 smoothing points were applied to all averaged raw spectra to allow visualization of important peaks.

Machine learning

Raw spectral signatures were organized in MS Excel spreadsheet before they were imported for analysis using JMP version 16.2 software (SAS institute, North Carolina, NC, USA). Data in excel spreadsheet were classified according to patient ID, infection status, parasitemia level, and *Plasmodium* species type.

In JMP, supervised machine learning was used to analyze the data. Data from infected patients were pooled regardless of the *Plasmodium* parasite they were infected with, their parasitemia level and the body part scanned. This allowed us to assess the capacity of NIRS to differentiate malaria infected from uninfected subjects regardless of their parasitemia level. As there was not enough *P. falciparum* infected samples to train a model for predicting *Plasmodium* species, we did not attempt to differentiate patients infected with *P. vivax* from those infected with *P. falciparum*. Spectra was first divided into a training set consisting 60% of all the data containing 216 spectral signatures from 16 malaria-positive and 20 malaria-negative subjects and the resultant model was used to predict an independent set of 11 malaria-positive and 13 malaria-negative subjects. We applied the model screening feature to simultaneously fit several machine learning algorithms, including Support Vector Machines, Decision Tree, K Nearest Neighbors, Bootstrap Forest, Boosted Tree, Discriminant, Logistic Regression, Artificial Neural Network (ANN), and Fit Stepwise on the data to allow us to compare and select the best predictive model for infection prediction using unique spectral peaks identified. Malaria infection status was used as the response factor and the identified unique spectral signatures for malaria, skin color, age, height, weight, body part scanned, and gender were used as predictors. The best predictive model selected for differentiating infected from uninfected samples was ANN. The ANN networks were fully connected, consisting of an input layer with the prior identified unique peaks, and an output layer. Activation between nodes was performed using the TanH function. The output layer was trained as a binary outcome (e.g., infected vs. uninfected). The resultant model was applied to predict individuals that were left out of the model.

Results

Results from PCR confirmed 45% ($N = 27$) of the 60 people scanned were positive with malaria, while the rest were malaria negative. Of the malaria-positive individuals, 75% ($N = 20$) and 25% ($N = 7$), were infected with *P. vivax* and *P. falciparum,* respectively. Results from microscopy indicated that out of the 27 infected patients, 7.4% (2 subjects) had extremely high parasitemia, 18.5% (5 subjects) had moderate parasitemia, 44.4% (12 subjects) had low parasitemia, and 29.6% (8 subjects) had very low parasitemia. Malaria positive and negative groups consisted of 60% and 66% women, respectively. Of those subjects that were malaria positive, their age ranged between 19 and 73 y old with 66% of them ≤40 y old whereas the age of the malaria-negative subjects ranged from 20 to 75 y old with 55% of them ≤40 y old. Out of the total, 70% of

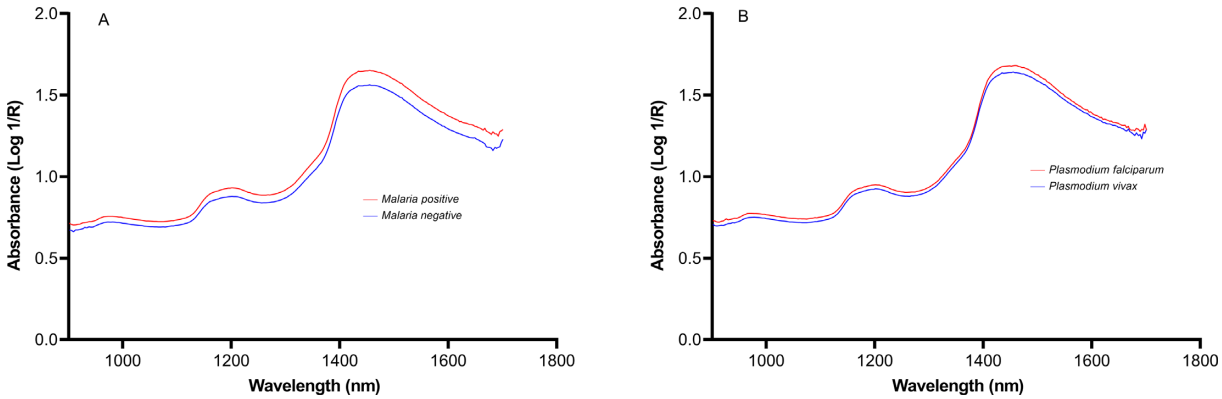

Figure 2. Raw average spectra of (A) malaria-positive and malaria-negative subjects irrespective of the *Plasmodium* species they were infected with and (B) *P. falciparum* and *P. vivax* infected patients.

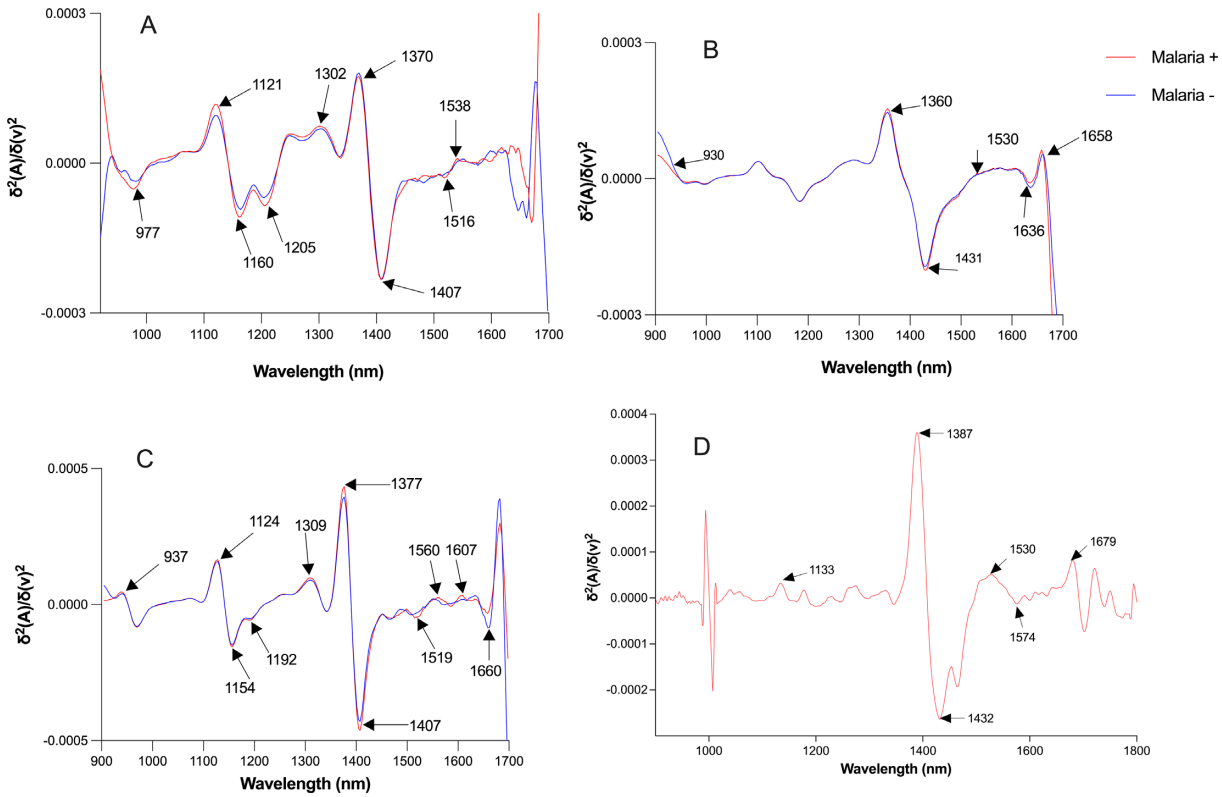

Figure 3. Second derivative spectra showing absorption peaks for malaria positive (red line) and negative (blue line) individuals collected from the ear (A), finger (B), arm (C), and purified *P. falciparum* (D). Spectra presented for A to C is an average of 27 infected subjects and 33 negative subjects.

malaria-negative subjects and 80% of malaria-positive subjects weighed under 70 kg.

Raw absorbance spectra

Absorption differences were seen from the raw spectra collected from malaria-positive and malaria-negative patients. Malaria-positive patients were generally seen to have higher absorbance values than malaria-negative patients. Similarly, patients with *P. falciparum* generated spectra with higher absorbance values relative to those that were infected with *P. vivax* (Fig. 2).

Absorption peaks for malaria-infected patients

Using the second derivative spectra of the ear, finger, and arm, absorption differences between malaria-positive and malaria-negative subjects were observed (Fig. 3). Spectra from the ear produced the most distinct bands whereas less distinct bands were seen from spectra collected from the arm. Distinct absorption peaks for malaria-positive patients were observed within the 1st to 3rd overtone regions and these bands were present in at least two body parts scanned. They include absorption peaks around 937, 1120, 1160, 1200, 1300, 1370, 1407, 1516, 1538, 1560, 1607, and 1660 nm (Fig. 3). Among them, those that were reduced in malaria-infected patients include peaks around 977, 1160, 1205, 1407, and 1516 nm whereas absorption peaks that increased in malaria-infected patients include those around 1120, 1300, 1538, 1560, and 1607 nm. Peaks in the second overtone region are dominated by overtones of O–H, N–H, and C=H combinations whereas the absorption peaks around 1400 to 1660 nm in the first overtone

Table 1. Unique malaria parasite peaks identified in this study, their bond vibration characteristics, and the structure as described in literature [24, 25].

Peak identified*	Bond vibration	Structure
930,937	C–H third overtone	CH_3
1121,1127	C–H second overtone	Lipids
1154,1160,1170	C–H stretch second overtone	CH_3 groups
1192,1205	C–H stretch second overtone	CH_3, Hemoglobin
1302,1309	C–H overtones and combinations	Fats/oils
1356,1368, 1370,1377	C–H stretch first overtone	CH_3 groups
1407,1413, 1421,1431	O–H first overtone	ROH Oil
1516,1519	N–H stretch first overtone	Protein
1530,1538	O–H stretch first overtone N–H	Starch
1560,1569	N=H stretch first overtone	CONH
1607	N=H stretch first overtone	
1636,1640, 1642	N=H stretch first overtone	Malaria hemozoin protein
1658,1660	C–H first overtone	Polyunsaturated fatty acid

Other peaks that were analogous to those described in the table but have not been described in literature are shown in Figs. 3 and 4.

region are dominated by C=H and O–H compounds related to parasite proteins (Table 1).

Absorption peaks for *P. falciparum* and *P. vivax*

Similarly, spectra from the ear produced the most distinct peaks for *P. falciparum* and *P. vivax*. The second derivative spectra of *P. falciparum* and *P. vivax* infected patients from the ear indicates that across the entire spectrum, distinct peaks for patients with *P. falciparum* parasites and *P. vivax* were around 960,1170, 1413,1474, 1569, 1538, and 1642 nm. When the ear was scanned, peaks at 960,1170, 1413, and 1538 nm were observed and these peaks were reduced in *P. vivax* infected subjects. Contrary, when the finger was scanned, peaks at 960 and 1474 nm increased in absorbance in *P. vivax* infected patients. The absorption peaks observed for the two species were also responsible for differentiating infected from uninfected subjects (see Fig. 3). Table 1 shows an average of all peaks identified that could be related to the presence of *Plasmodium* parasites.

Change of absorption peaks with parasitemia

The absorbance peaks of infected subjects were compared against parasitemia levels as well as against peaks from malaria-negative subjects. The absorbance at 960 nm was lowest and highest for patients with very high parasitemia and malaria-negative patients, respectively. The absorption peaks at 1110 and 1290 nm were highest for patients with very low parasitemia but lowest for subjects that were malaria negative whereas the peak at 1180 nm was lowest for subjects with very low parasitemia but highest for malaria-negative patients. Generally, absorption peaks were stable across patients with low and high parasitemia (Fig. 5).

Sensitivity, specificity, and accuracy of NIRS

We tested on a preliminary scale whether the identified absorption peaks could predict infected and uninfected subjects using ANN machine learning models. Spectra collected from the ear produced the most accurate prediction of infection in the independent subjects with an accuracy of 92% ($N = 24$), sensitivity of 100% ($N = 11$) and specificity of 85% ($N = 13$). Moreover, sensitivity was 100% across all parasitemia levels. Sensitivity and specificity were similar between replicate body parts scanned indicating the spectra was collected with minimal errors between the left and right body parts. Comparatively, the accuracy, sensitivity, and specificity of the spectra collected from the finger was 70% ($N = 24$), 72 ($N = 11$), and 69% ($N = 13$), respectively, whereas spectra of the arm resulted into a predictive accuracy of 72% ($N = 24$), sensitivity of 59% ($N = 11$), and specificity of 85% ($N = 13$). Figure 6 shows a summary of the differentiation of infected and uninfected patients based on the spectra of the ear alone.

Discussion

We assessed whether a rapid, non-invasive, and reagent-free technique that uses the near-infrared region of the electromagnetic spectrum could produce unique malaria spectral signatures and if those signatures could be applied to predict malaria infection status in human subjects. The spectral signatures collected from 27 malaria-positive individuals, regardless of (1) their parasitemia level and (2) whether they were positive with *P. falciparum* or *P. vivax*, were seen to be different from signatures of the 33 malaria-negative individuals. The spectra from the ear produced the most distinct bands for the two groups. Similarly, remarkable albeit few differences were observed for spectral signatures of subjects that were infected with *P. falciparum* and *P. vivax* indicating their chemical profile could be different. When these unique signatures were applied to differentiate infected from uninfected subjects, sensitivity of 100% and accuracy of 92% were achieved using spectra collected from the ears.

We hypothesized that the invasion of *Plasmodium* parasites into the human host's red blood cells results in significant structural, biochemical, and functional changes that generate unique infrared absorption peaks for malaria-positive and -negative individuals. This include the loss of the discoid shape of the red blood cells, reduced hemoglobin concentration, increased adhesiveness and permeability to *Plasmodium* species infection [26]. In addition, over 400 *Plasmodium* parasite-related proteins, including the commonly used biomarker for malaria infection, i.e., the hemozoin protein, hydroxy fatty acids, and lipids, are released into red cells [27–29]. These molecules can absorb light at specific wavelengths to generate unique absorption bands that could be used as biomarkers for malaria infection (Fig. 3). We also tested whether *P. vivax* and *P. falciparum* cause remarkable differences to host red cells resulting into a unique NIR spectrum. For example, it has been reported that an infection with *P. vivax* results in enlarged, pale, fine stippling parasitized red cells known as Schuffener's dots [30], whereas infection with *P. falciparum* results in fine stippling non-enlarged parasitized cells known as Maurer's clefts [31]. There are also remarkable genomic and structural differences between schizonts, trophozoites, and gametocytes of the two species that are expected to generate unique infrared spectral signatures [32].

The infrared absorption peaks for malaria identified in this study through non-invasive scanning were consistent with peaks observed when pure *P. falciparum* parasites were scanned (Fig. 3D). The peaks in our study were also consistent with peaks reported by two previous studies that used NIRS to detect *P. falciparum* and hemoglobin in red blood cells *in vitro* [33, 34]. To our knowledge, this is the first study to report unique NIR absorption peaks for

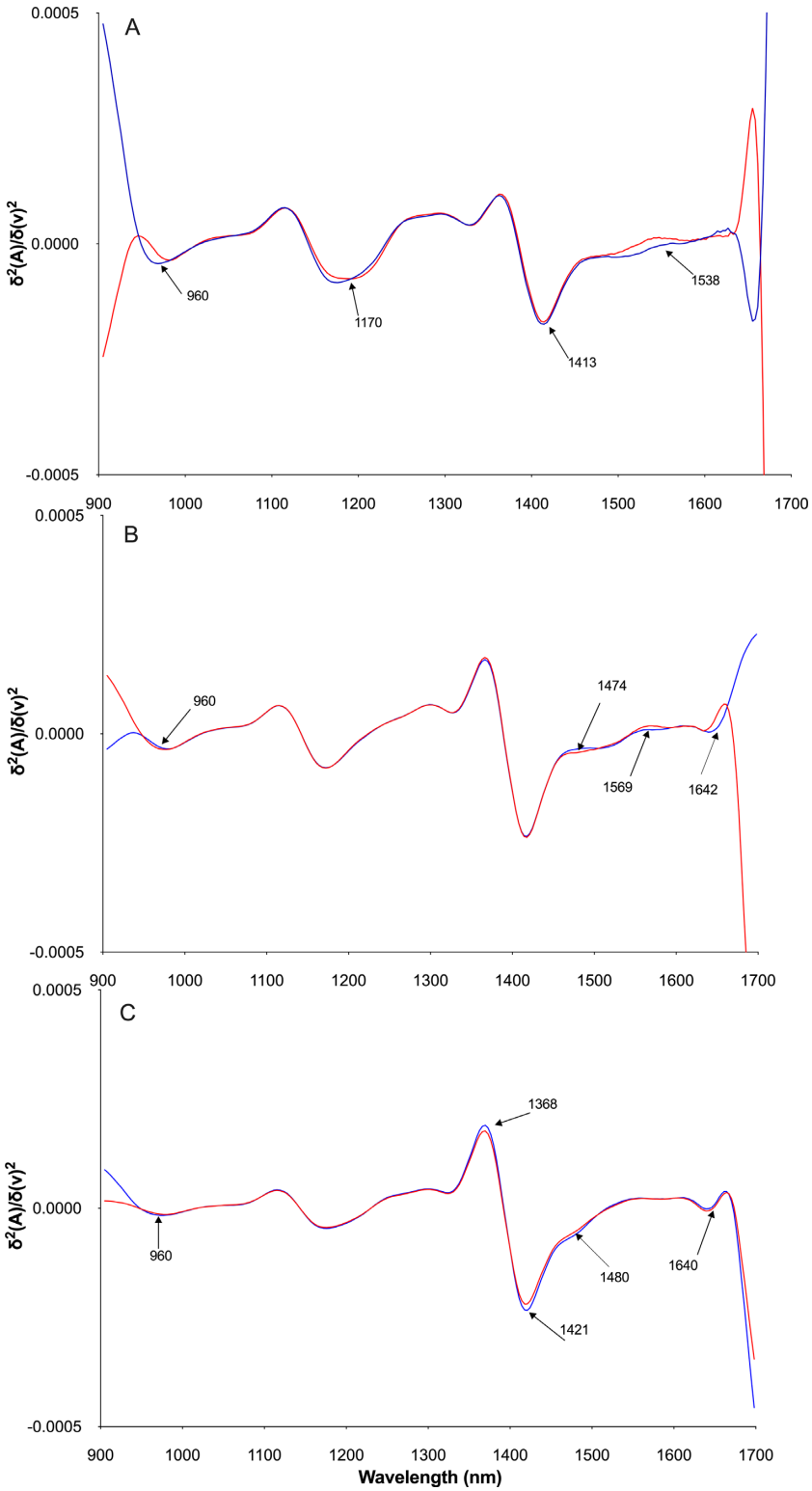

Figure 4. Second derivative spectra showing absorption peaks for *P. falciparum* (red line) and *P. vivax* (blue line) for the spectra collected from the ear (A), finger (B), and arm (C). Spectra shown is an average of 7 *P. falciparum* and 20 *P. vivax* infected subjects.

malaria parasites acquired non-invasively through the skin of human subjects with diagnostic features. Our previous NIR studies have indicated that the technique can also non-invasively detect other infections in mosquitoes such as malaria [35], Zika [36], *Wolbachia* [37], and chikungunya [38]. NIRS has also been used to detect cancer tumors in patients [39–41].

When *Plasmodium* parasites consume hemoglobin in red blood cells, they produce a toxic compound known as heme. Heme is detoxified by the parasite into hemozoin pigment through metabolization of hemoglobin. Hemozoin is therefore considered a powerful and reliable biomarker for malaria infection. Using second derivative average spectra of malaria-positive and malaria-

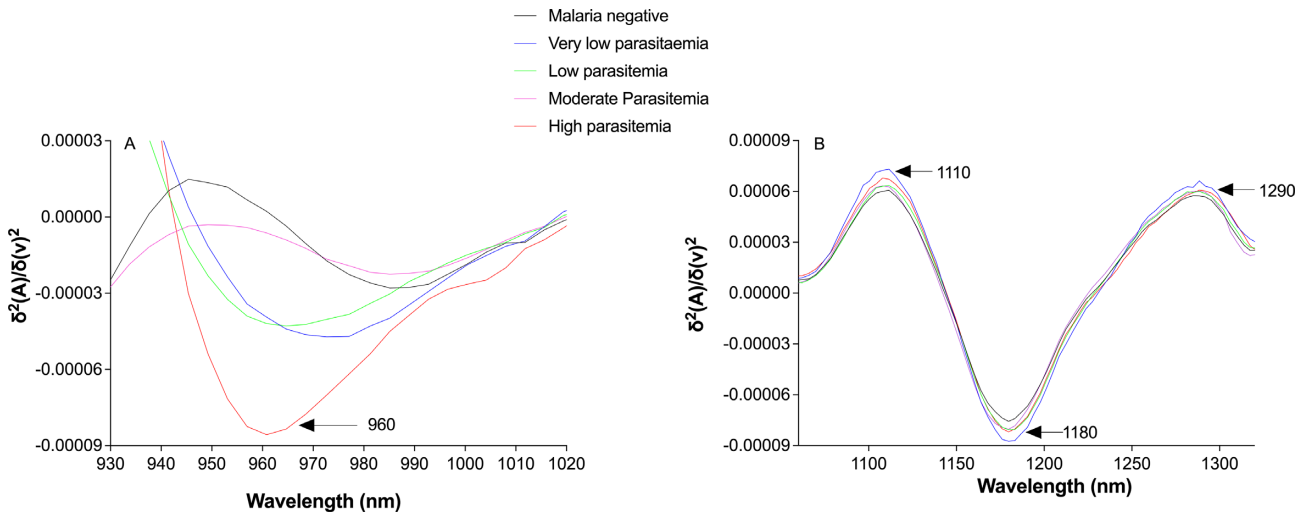

Figure 5. Absorption peaks of malaria-positive subjects with varying parasitemia relative to malaria-negative subjects using average spectra collected from the ear for a peak at 960 nm (A) and peaks at 1110,1180, and 1290 nm (B).

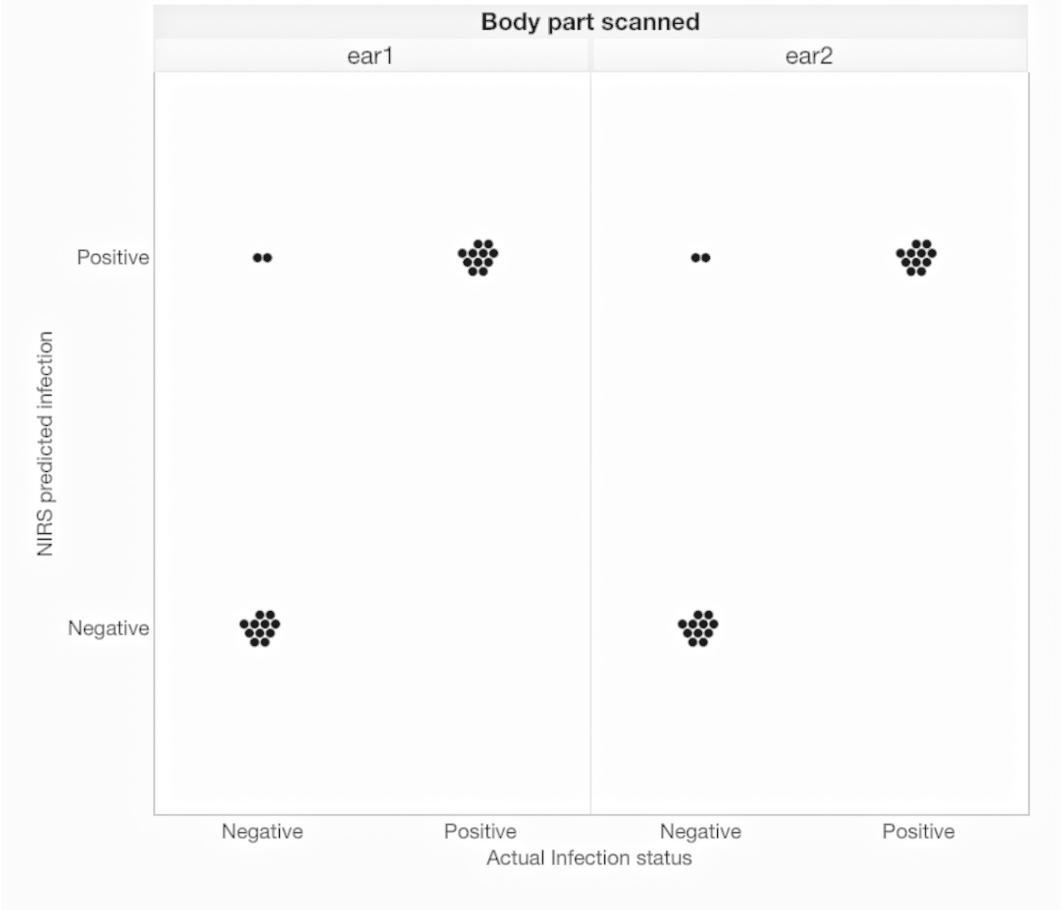

Figure 6. Results of the ANN model used to differentiate infected and uninfected subjects who were used to validate the model. Each circle represents one subject and results shown are for scans of the left ear (ear1) and the right ear (ear2) of each patient.

negative patients, we observed several bands that have previously been reported as hemozoin absorption bands. Figure 3 shows absorption bands around 1505 to 1560 nm, 1636 to 1642 nm, and 1515 nm previously observed from synthetic hemozoin (β-hematin) and dry hemozoin isolated from infected red blood cells [33]. Absorption bands around 1205, 1431, and 1642 nm in the second overtone region are related to hemoglobin as reported by Kuenstner and Norris [34] and more recently by Adegoke and colleagues [33]. Absorption bands around 1432 and 1388 nm were observed when pure *P. falciparum* parasites were scanned (Fig. 3D). In this study, hemoglobin bands around 1205 nm and bands around 1400 to 1431 nm were reduced in malaria positive individuals. A

reduction in hemoglobin concentration is expected for a malaria-infected patient as the presence of the malaria parasite consumes hemoglobin and other red blood cell proteins to produce heme.

Current malaria elimination strategies require high-throughput approaches that can facilitate cost-effective, rapid, and large-scale surveillance of malaria cases. Here, we have identified unique peaks for malaria parasites and have gone a step further to show that the peaks could differentiate infected from uninfected malaria subjects with low and extremely high parasitemia providing the first evidence of the potential use of an affordable, light-based technology for rapid and non-invasive surveillance of malaria in large-scale programmatic studies. By removing the need to draw blood, non-invasive surveillance of malaria by NIRS has the potential to revolutionize our ability to rapidly detect malaria in large-scale human populations and facilitate timely treatment to reduce further transmission. With a sensitivity of 100% achieved at very low parasitemia, NIRS could enable rapid large-scale screening of communities to identify asymptomatic patients and make malaria diagnosis among babies a painless undertaking. Following the development of predictive models, NIRS could enable thousands of individuals to be screened in a day with unskilled personnel. Furthermore, the spectrometer used for this study allows cloud-based prediction for real-time monitoring of malaria infections among large-scale community groups and in multiple locations including in rural areas. Cloud-based and real-time surveillance means data will be available to decision-makers in real time, thereby facilitating rapid decision-making and timely distribution of resources where required to stop further transmission and outbreaks.

Furthermore, NIRS is a unique tool that could facilitate timely isolation and treatments of infected cases, through mass screening of populations at risk, including at ports of entry such as airports or even at household levels, to stop transmission to local mosquito populations by overseas travellers, reduce global outbreaks, and prevent reintroduction in areas under elimination. The NIRS unit that was assessed under this study is an off-the-shelf spectrometer that could easily be integrated and scaled up into existing programmatic malaria epidemiological surveillance programs. However, further work is recommended on a larger scale in multiple malaria epidemiological settings to develop robust predictive models. Factors such as malaria species type, asymptomatic malaria cases, age groups, blood groups, skin color, and most importantly the presence of mixed/co-infections of malaria species or other pathogens should be considered in future studies for developing robust malaria-specific predictive models. Future work should also assess the capacity of the tool to quantify parasitemia of infected individuals and ability to differentiate subjects infected with different *Plasmodium* species.

In conclusion, our proof-of-concept study provides insights into the potential application of NIRS and machine learning techniques for rapid, non-invasive, and large-scale surveillance of malaria and potentially other human pathogens.

Acknowledgments

We thank Aline Tatila-Ferreira, Lilha M.B. dos Santos, and Edson Dantas for technical support.

Funding

The work was funded by Fiocruz INOVA Ideias Inovadoras, Conselho Nacional de Pesquisa e Desenvolvimento Científico e Tecnológico, Fundação Carlos Chagas Filho de Amparo a Pesquisa do Estado do Rio de Janeiro, Advance Queensland Industry Research Fellowship (AQIRF2018019 awarded to M.T.S.-L), and the NHMRC project grant (APP1159384 awarded to M.T.S.-L).

Authors' Contributions

G.A.G.: study design, human data collection, and PCR test; T.N.K.: data curation; A.R.L.: study design and model design; C.F.C., L.B.C., and J.C.L.-J.: study design and data collection; R.M-d-F.: study design and funding; and M.T.S.-L.: study design, data analysis, manuscript writing, and funding. All authors read and approved the final manuscript.

Data Availability

Anonymized patient data used in this study are available at https://doi.org/10.48610/e19e6fc.

References

1. WHO. 2021. World malaria report. Geneva, Switzerland: World Health Organization.
2. WHO. 2015. Global technical strategy for malaria 2016–2030. Geneva, Switzerland: World Health Organization.
3. Lin JT, Saunders DL, Meshnick SR. 2014. The role of submicroscopic parasitemia in malaria transmission: what is the evidence? Trends Parasitol 30(4):183–190.
4. Sturrock HJ, *et al.* 2013. Targeting asymptomatic malaria infections: active surveillance in control and elimination. PLoS Med 10(6):e1001467.
5. Warhurst D, Williams J. 1996. ACP Broadsheet No 148. July 1996. Laboratory diagnosis of malaria. J Clin Pathol 49(7):533.
6. Mwangi TW, *et al.* 2005. Clinical algorithms for malaria diagnosis lack utility among people of different age groups. Trop Med Int Health 10(6):530–536.
7. Berzosa P, *et al.* 2018. Comparison of three diagnostic methods (microscopy, RDT, and PCR) for the detection of malaria parasites in representative samples from Equatorial Guinea. Malar J 17(1):333.
8. Payne D. 1988. Use and limitations of light microscopy for diagnosing malaria at the primary health care level. Bull World Health Organ 66(5):621.
9. Moody A. 2002. Rapid diagnostic tests for malaria parasites. Clin Microbiol Rev 15(1):66–78.
10. Cunha CB, Cunha BA. 2008. Brief history of the clinical diagnosis of malaria: from Hippocrates to Osler. J Vector Borne Dis 45(3):194–199.
11. Murray CK, *et al.* 2003. Rapid diagnostic testing for malaria. Trop Med Int Health 8(10):876–883.
12. Rubio J, *et al.* 2001. Limited level of accuracy provided by available rapid diagnosis tests for malaria enhances the need for PCR-based reference laboratories. J Clin Microbiol 39(7):2736–2737.
13. McMorrow ML, Aidoo M, Kachur SP. 2011. Malaria rapid diagnostic tests in elimination settings—can they find the last parasite? Clin Microbiol Infect 17(11):1624–1631.
14. Humar A, *et al.* 1997. ParaSight F test compared with the polymerase chain reaction and microscopy for the diagnosis of *Plasmodium falciparum* malaria in travelers. Am J Trop Med Hyg 56(1):44–48.
15. Brown AE, *et al.* 1992. Demonstration by the polymerase chain reaction of mixed *Plasmodium falciparum* and *P. vivax* infections

undetected by conventional microscopy. Trans R Soc Trop Med Hyg 86(6):609–612.
16. Morassin B, *et al.* 2002. One year's experience with the polymerase chain reaction as a routine method for the diagnosis of imported malaria. Am J Trop Med Hyg 66(5):503–508.
17. Patsoula E, *et al.* 2003. A single-step, PCR-based method for the detection and differentiation of *Plasmodium vivax* and *P. falciparum* Ann trop med parasitol 97(1):15–21.
18. WHO. 2000. New perspectives: malaria diagnosis. Report of a Joint WHO/USAID Informal Consultation, 25–27 October 1999. [accessed 2021 Dec 15]. https://apps.who.int/iris/bitstream/handle/10665/66321/WHO_CDS_RBM_2000.14.pdf.
19. Oliveira-Ferreira J, *et al.* 2010. Malaria in Brazil: an overview. Malar J 9(1):1–15.
20. Epidemiológico B 2020. Secretaria de Vigilância em Saúde /Ministério da Saúde Número Especial Nov. 2020 (ISSN 9352-7864). [accessed 2021 Dec 15]. https://www.gov.br/saude/pt-br/centrais-de-conteudo/publicacoes/boletins/epidemiologicos/especiais/2020/boletim_especial_malaria_1dez20_final.pdf.
21. Snounou G, *et al.* 1993. High sensitivity of detection of human malaria parasites by the use of nested polymerase chain reaction. Mol Biochem Parasitol 61(2):315–320.
22. Snounou G, Singh B. 2002. Nested PCR analysis of *Plasmodium* parasites. Methods Mol Med 72:189–203.
23. Savitzky A, Golay MJ. 1964. Smoothing and differentiation of data by simplified least squares procedures. Anal Chem 36(8):1627–1639.
24. Weyer L. 2007. Practical guide to interpretive near-infrared spectroscopy. Boca Raton, Florida: CRC press.
25. Burns DA, Ciurczak EW. 2007. Handbook of near-infrared analysis. Boca Raton, Florida: CRC press.
26. Mohandas N, An X. 2012. Malaria and human red blood cells. Med Microbiol Immunol (Berl) 201(4):593–598.
27. Hiller NL, *et al.* 2004. A host-targeting signal in virulence proteins reveals a secretome in malarial infection Science 306(5703):1934–1937.
28. Pandey AV, *et al.* 2003. Hemozoin formation in malaria: a two-step process involving histidine-rich proteins and lipids. Biochem Biophys Res Commun 308(4):736–743.
29. Schwarzer E, *et al.* 2003. Malaria-parasitized erythrocytes and hemozoin nonenzymatically generate large amounts of hydroxy fatty acids that inhibit monocyte functions. Blood 101(2):722–728.
30. Barnwell JW, *et al.* 1990. *Plasmodium vivax*: malarial proteins associated with the membrane-bound caveola-vesicle complexes and cytoplasmic cleft structures of infected erythrocytes. Exp Parasitol 70(1):85–99.
31. Lanzer M, *et al.* 2006. Maurer's clefts: a novel multi-functional organelle in the cytoplasm of *Plasmodium falciparum*-infected erythrocytes. Int J Parasitol 36(1):23–36.
32. Das A, *et al.* 2009. *Plasmodium falciparum* and *Plasmodium vivax*: so similar, yet very different. Parasitol Res 105(4):1169–1171.
33. Adegoke JA, *et al.* 2021. A near-infrared "matchbox size" spectrometer to detect and quantify malaria parasitemia. Anal Chem 93(13):5451–5458.
34. Kuenstner JT, Norris KH. 1994. Spectrophotometry of human hemoglobin in the near infrared region from 1000 to 2500 nm. J Near Infrared Spectrosc 2(2):59–65.
35. Maia MF, *et al.* 2019. Detection of *Plasmodium falciparum* infected *Anopheles gambiae* using near-infrared spectroscopy. Malar J 18(1):1–11.
36. Fernandes JN, *et al.* 2018. Rapid, noninvasive detection of Zika virus in *Aedes aegypti* mosquitoes by near-infrared spectroscopy. Sci Adv 4(5):eaat0496.
37. Sikulu-Lord MT, *et al.* 2016. Rapid and non-destructive detection and identification of two strains of Wolbachia in *Aedes aegypti* by near-infrared spectroscopy. PLoS Negl Trop Dis 10(6): e0004759.
38. Santos LM, *et al.* 2021. High throughput estimates of Wolbachia, Zika and chikungunya infection in Aedes aegypti by near-infrared spectroscopy to improvearbovirus surveillance. Commun Biol 4(1):1–9.
39. Xue Z, Zeng S, Hao J. 2018. Non-invasive through-skull brain vascular imaging and small tumor diagnosis based on NIR-II emissive lanthanide nanoprobes beyond 1500 nm. Biomaterials 171:153–163.
40. Kondepati VR, Heise HM, Backhaus J. 2008. Recent applications of near-infrared spectroscopy in cancer diagnosis and therapy. Anal Bioanal Chem 390(1):125–139.
41. Abe K, *et al.* 2013. Non-invasive *in vivo* imaging of near infrared-labeled transferrin in breast cancer cells and tumors using fluorescence lifetime FRET. PLoS One 8(11):e80269.